

Dynamics of Mass Transport and Magnetic Fields in Low-Wire-Number-Array Z Pinches

V. V. Ivanov,¹ V. I. Sotnikov,¹ G. S. Sarkisov,² T. E. Cowan,¹ S. N. Bland,³ B. Jones,² C. A. Coverdale,² C. Deeney,²
P. J. Laca,¹ A. L. Astanovitskiy,¹ and A. Haboub¹

¹University of Nevada, Reno, 5625 Fox Ave, Reno, Nevada 89506, USA

²Sandia National Laboratories, Albuquerque, New Mexico 87110, USA

³Blackett Laboratory, Imperial College, London SW7 2BZ, United Kingdom

(Received 3 July 2006; published 18 September 2006)

The dynamics of mass transport were observed in a wire array implosion with multiframe laser probing. Plasma bubbles arise at breaks in the wires. Interferometry shows that the leading edge of the bubbles brings material to the axis of the array. The speed of this material was measured to be $\geq 3 \times 10^7$ cm/s during the wire array implosion. A shock was observed during the collision of the bubbles with the precursor. The Faraday effect indicates current flowing in breaks on the wires. The current switches from the imploding mass to the on-axis plasma column at the beginning of the x-ray pulse.

DOI: [10.1103/PhysRevLett.97.125001](https://doi.org/10.1103/PhysRevLett.97.125001)

PACS numbers: 52.59.Qy, 52.58.Lq

Multi-Mega-Ampere Z pinches are powerful laboratory sources of x-ray radiation that have been applied to fusion research and other areas of dense plasma physics [1,2]. Wire array physics investigations have shown fast progress in recent years, linked to the study of implosion dynamics, instabilities, and 3D structures in wire array z pinches [3–6].

Experiments have demonstrated that the implosion dynamics of wire arrays differ from the implosion dynamics of annular plasma shells [4,6–10]. The wires remain at their initial positions in the array for the first 50%–80% of the time of implosion, and the primary implosion begins when breaks arise on the wires. A snowplowlike model of implosion was suggested in Refs. [8,9], where a shock during implosion was seen by x-ray diagnostics. In works [4,5,11], new details of the implosion phase were observed by optical and x-ray probing. A broad radial mass distribution during implosion was seen in wire arrays at the 20 MA Z facility [3], where part of the wire mass did not implode and produced trailing mass at stagnation. Similar observations were also made at 1–3 MA facilities [4,6,7]. “Bubbles” in plasma streams formed at the start of implosion have been observed at different pulsed power generators as well [4,10–12]. The nonuniform ablation and formation of bubbles at wire radius discontinuities was observed in Ref. [13]. Development of induced bubbles was investigated with a gated extreme ultraviolet (XUV) pinhole camera. Discontinuities in the wire diameter induced bubbles which initiated the implosion sooner than in the regular wire array [13].

In this Letter, the detailed dynamics of mass transport and current in low number wire arrays are described. We show that bubbles in plasma streams present a method of mass transport in wire arrays. In the Zebra generator bubbles were observed in experiments studying the implosion of Al, Cu, Ti, and W wire array loads. Development of plasma bubbles at gaps formed in the ablating wires, movement of material to the axis, and shock in the precursor

were investigated in Al loads. Interferometry reveals that the leading edge of the bubbles brings material from wires to the axis during the implosion. The speed and acceleration of material during the implosion was measured. We show for the first time that current flows through the wire gaps, and current in jets that extend from the bubbles to the precursor formed on axis. The observed implosion dynamics are compared with experiments carried out on the MAGPIE generator.

The experiments were carried out on the Zebra generator, which produces a 1 MA current pulse with a rising edge of ~ 80 ns. Plasma diagnostics include five-frame laser probing of the Z pinch in three directions [10]. Four frames of the shadowgraphy cover two probing directions. The third probing direction includes shadowgraphy, Faraday rotation diagnostics, an interferometer, and schlieren diagnostics all at one temporal location. A short 150 ps laser pulse provides instant images of the fast moving plasma on CCD cameras. A “long” (34 ns) train or a “short” (9 ns) train of equidistant laser pulses was used for probing. Temporal profiles of the x-ray pulses were recorded with filtered photo-conducting detectors. The experiments were carried out with 2 cm tall, 1.6 cm diameter Al wire arrays. Two load configurations were fielded: 8 wires, 15 μm diameter (37 $\mu\text{g}/\text{cm}$) and 4 wires, 20 μm diameter (33 $\mu\text{g}/\text{cm}$). While high wire number is important in producing high x-ray power [1,2,6] these regimes are not accessible on 1 MA facilities. However, the same basic ablation and implosion dynamics is observed from 1–20 MA [3,6]. The 4-wire experiments certainly are not optimized for x-ray production, but they allow a clear view of the wire dynamics from the initial position to the array axis, and which are expected to be relevant to instability evolution in higher wire number arrays as well.

The early stage of the implosion phase in an Al 8-wire array is presented in Fig. 1. Two frames of the shadowgraphy from one probing direction are separated by 7 ns. Jets with the period ~ 0.4 mm flow out from lobes on the

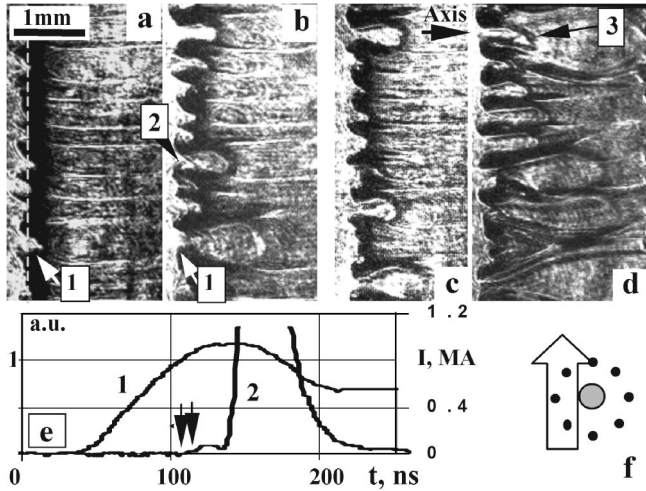


FIG. 1. Two frames of the shadowgraphy (a), (b) and (c), (d) from shots 511 and 514, the timing diagram (e) from shot 511, and the direction of probing in Al 8-wire arrays (f). The delay between frames is 7 ns. Arrows in diagram (e) present a temporal position of frames (a), (b): (1) is the current pulse and (2) is the x-ray pulse.

plasma column around the wire, as shown in Fig. 1(a). Breaks or gaps in the wire cores arise at locations with smaller diameter or waists. Material is thought to flow axially out of the waist regions [14]. In Figs. 1(a) and 1(b), the arrows labeled (1) show development of the implosion bubble from the wire break. Bubbles in the plasma streams suggest a burnout of the wire cores and the beginning of the implosion phase, as suggested in Ref. [8]. In the 8-wire arrays, breaks on the wire arise ~30 ns before the start of the x-ray pulse, are seen in Fig. 1(e). Figures 1(c) and 1(d) highlight the development of the bubbles. The average speed of the leading edge of the bubbles was calculated from the shadowgrams, discussed in Fig. 3 below. In Fig. 1(b), the arrow labeled (2) shows plasma beginning to span the break on the wire. Arrow (3) shows plasma blown from the gap toward the axis as a secondary bubble, which indicates current across the wire break.

In Fig. 2(a), the interferogram from an 8-wire array is shown. The leading edges of the bubbles deliver material from the wire to the axis. This leading edge can accrete

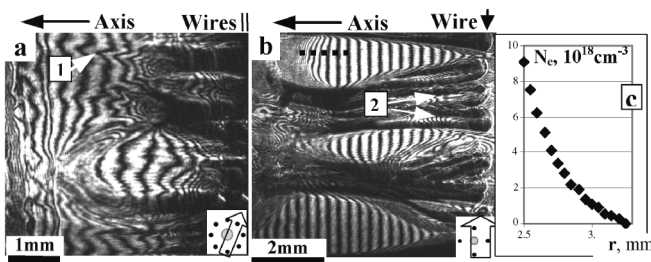


FIG. 2. Interferograms from 8-wire (a) and 4-wire (b) Al arrays from shots 519 and 541 and the diagram of the electron plasma density (c) calculated along the dotted line on panel (b).

ablated plasma filling the array before the beginning of implosion stage. Plasma streams from two wires overlap in the image shown in Fig. 2(a); therefore the four-wire loads with a clear inward view from the edge to the axis of the array were used for the detailed investigation of mass transport. The arrows labeled (2) in Fig. 2(a) point to “fingers” of trailing material. A significant portion of the plasma resides in these structures. This material forms extended streams of the trailing mass [3,4]. The Fig. 2(c) shows that the plasma density on the leading edge of the bubble from Fig. 2(b) is $n_e > 10^{19} \text{ cm}^{-3}$. The plasma density inside the large bubbles is below the sensitivity of the interferometer, $n_e < 8 \times 10^{17} \text{ cm}^{-3}$.

The average radial speed of the leading edge of bubbles during 7 ns, as measured from the shadowgrams on the same probing direction, is plotted in Fig. 3(a) as a function of the initial radial size Δr of the bubble. The speed of the material was measured to be $(2-3.5) \times 10^7 \text{ cm/s}$ in the 8-wire arrays and $(2-6) \times 10^7 \text{ cm/s}$ in the 4-wire arrays. An acceleration of $(2.5-5) \times 10^{15} \text{ cm/s}^2$ was measured in these same wire arrays in the beginning of bubbles movement. Large variation of the speed is seen on the diagram in Fig. 3(a). Several sources of variation for the bubble parameters were identified. First, the core of the wire is burnt out stochastically and bubbles start growing at different times. Second, the bubbles from one wire can have different speeds. Third, large variations in speed are seen from wire to wire within an array. Variation of bubble parameters leads to a distribution of material arriving to the axis, with a total delay of ~15–20 ns from the beginning to the end. The delay between the first and the last bubbles reaching the axis may be responsible for the duration of the rising edge of the generated x-ray pulse. Indeed, the rise time of the x-ray pulse in 8-wire Al arrays is 15–25 ns on the Zebra generator [10]. The main x-ray pulse begins when bubbles bring material and kinetic energy to the precursor. X-ray radiation was observed in Ref. [13] when bubbles from induced discontinuities reached the axis of the array. Plasma residing in the trailing mass reaches the axis after the maximum of the radiated x-ray pulse, as observed at high wire number experiments [3,6].

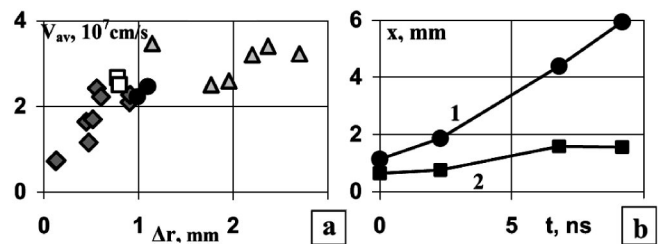


FIG. 3. (a) Dependence of the average speed of the leading edge on the initial radial size of bubbles from three shots with Al 8-wire arrays. (b) Dependence of the radial (1) and axial (2) size of bubbles with time. Every point is averaged for 4 bubbles from one wire in shot 540.

Four frames of the shadowgraphy were analyzed to measure acceleration of material imploding from one wire in the 4-wire array. The leading edges of bubbles were identified and tracked in the four images. Average results for four bubbles with similar initial size are presented in plots (1) and (2) in Fig. 3(b). It is seen in diagram (1) that the leading edge of the bubbles accelerates mainly in the beginning of movement, over several nanoseconds. The acceleration is reduced, or absent, in the last half of the implosion. An axial expansion of bubbles presented in diagram (2) also shows acceleration in the beginning of movement. Saturation of the axial expansion occurs when sides of the neighboring bubbles merge.

The Faraday rotation diagnostic [15,16] was applied to study magnetic fields and current during implosion. Polarizers in the Faraday channel were mismatched at 3° to differentiate directions of the rotation of the polarization plane. Jets flowing from the leading edge of the bubble to the precursor were seen on the interferograms and schlieren images. The Faraday effect indicates radial current in these jets. Faraday and schlieren images also show jets in bubbles flowing out from the gap in the wire.

Complementary pairs of the Faraday image and the shadowgram show the Faraday effect in Fig. 4. The shadowgram in Fig. 4(a) shows a collision of the bubbles with the precursor. The edge of the undisturbed precursor is seen in the middle of the shadowgram where the bubble has not yet reached the edge of the precursor. Bubbles in the top and in the bottom of the image collide with the precursor at a speed $\geq 3 \times 10^7$ cm/s. Lineouts in Fig. 4(c) from the shadowgram show that the bubbles colliding with the

precursor have steep leading edges. The Alfvén velocity, V_A , in the Al plasma column, with the electron density $n_e = 10^{19}$ cm $^{-3}$ and $B = 0.3$ MG [16] is $\sim 10^7$ cm/s. The speed of sound, V_s , in this plasma column is $\sim 0.5 \times 10^7$ cm/s. The measured speed of material during the implosion is 2–4 times more than V_A and V_s . Therefore collision of the bubbles with the precursor produces a shock. This shock can be an effective mechanism of plasma heating.

The Faraday image presented in Fig. 4(b) shows magnetic fields in the side edges of the bubbles and, presumably, illustrates a moment when current switches from the remnant plasma near the initial wire position to the precursor. The images of Fig. 4 were collected at the beginning of the main radiated x-ray pulse rise.

The observed dynamics of the mass transport helps to determine dominant physical mechanisms involved in the implosion. Plasma acceleration in bubbles can be produced by the Lorentz force of the global magnetic field and by the Amperian hoop force in the current-carrying plasma loop. The current in the precursor of Al 8-wire array was estimated as 0.1–0.2 MA [16], which suggests that the current in one wire is ~ 0.1 MA. Suppose a plasma column includes $\sim 70\%$ of the initial wire mass and is stretched in ~ 4 times in the bubble. Interaction of the magnetic field, created by the loop [17] with the current in the loop, gives rise to the Ampère force, which acts in the radial direction. For a plasma loop 1 mm of diameter with 0.1 MA current, the Ampère force produces plasma acceleration $\sim 4 \times 10^{15}$ cm/s 2 . The Lorentz force in the magnetic field of an 8-wire array, integrated by the Biot-Savart formula, produces plasma acceleration $\sim 1.3 \times 10^{15}$ cm/s 2 , which is smaller than the observed accelerations presented here. Together, these two forces can accelerate plasma to a speed of $\sim 3 \times 10^7$ cm/s during ~ 4 –6 ns, which is in agreement with experimental data. Before the formation of bubbles, discontinuities on the plasma column produce strong local magnetic field [5,12]. The Lorentz force creates initial curvature in the plasma column and predetermines the direction of plasma acceleration. The formation of a bubble at a wire core break is shown in Fig. 1(a) by arrow (1). In this region, the Lorentz force pushes plasma to the axis of the array and the plasma bubble is blown inward.

Acceleration of the leading front slows when the radial size of the bubble reaches 1–2 mm as shown in Fig. 3. It can be explained if the majority of the current switches back to remnant plasma at the initial position of the wire or if the bubble snowplows ablated plasma filling the array before the implosion stage. The Faraday diagnostic and secondary bubbles show that a significant part of current flows in plasma on the initial position of the wire. Plasma in gaps on the wire is seen on shadowgrams and interferograms. Plasma is blown from the gaps again by the Lorentz and Ampère forces. Arrow (2) in Fig. 1(d) points to a small secondary bubble inside the large bubble. A typical elec-

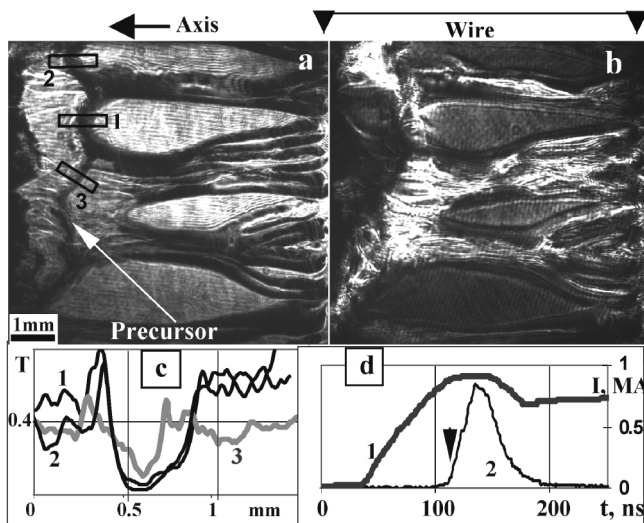


FIG. 4. The shadowgram (a), the Faraday image (b), and the timing diagram (d) of the implosion of the Al 4-wire array (shot 541). The arrow in diagram (d) represents the temporal position of the frame, (1) is the current pulse, and (2) is the x-ray pulse. Diagram (c) presents outlines from leading edges (1, 2) and the precursor (3) from the appropriate rectangles 1, 2, and 3 in the shadowgram (a).

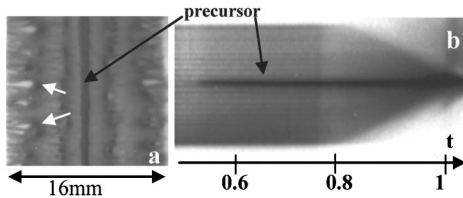


FIG. 5. (a) XUV framing imaging of 8×10 mm Cu array on MAGPIE, midway through implosion. (b) optical streak image of array, normalized to implosion time.

tron plasma density of $\sim 10^{19} \text{ cm}^{-3}$, with a radial size of 1–1.5 mm, was measured in the gap in the wire core of the 4-wire array by interferometry and could support current at this location. The Faraday diagnostic shows magnetic fields and current ≥ 0.1 MA across the wire break in the 4-wire array at a time near the current maximum.

Laser probing of Cu loads in the Zebra generator showed dynamics similar to the dynamics observed in the Al loads, but in the Cu wire arrays, plasma streams bring more material at the ablation stage. Bubbles snowplow ablated material and accretion of material could decelerate the leading edge of bubbles. Observed dynamics are similar in the implosion of 4–32 wires that leads to the assumption that this physics can be applied qualitatively to larger generators. Implosion bubbles become smaller and more regular in 24–32-wire arrays.

The implosion dynamics observed in the Zebra generator display similar plasma ablation and implosion mechanisms as those observed at the MAGPIE generator [4,18]. In MAGPIE experiments, loads with up to 64 wires are imploded from the same diameter as the Zebra experiments due to the longer current rise times and higher accumulated energy available for experiments. Prior to implosion, jets from the wires in MAGPIE experiments display an axial period of ~ 0.5 mm [8], similar to Zebra experiments [10]. Implosion in MAGPIE begins in the same manner as in Zebra experiments, with asymmetric ablation of the wire cores resulting in breaks and bubbles accelerating to the axis (Fig. 5). The MAGPIE implosion was recorded with optical streak photography and XUV framing images.

Like the Zebra probing images, the optical streaks in Fig. 5(b) show that the bubbles have an initial high acceleration, followed by a near constant velocity implosion at 0.85–1 on the x-axis. The XUV images show that the

bubbles rapidly increase in axial size and merge to form a spatial wavelength $\sim 4 \times$ the initial axial period. An increase in emission seen at the front of the bubbles is consistent with the accumulating mass that had been ablated from the wires prior to implosion. “Cleared out” regions are seen in the wake of the snowplow. The generally higher wire numbers in MAGPIE experiments often lead to the implosion of adjacent wires producing a snowplow sheath. As seen at the start and rise time of the x-ray pulse in Zebra experiments, the start and rise time of the x-ray pulse in the MAGPIE experiments coincide with the arrival of the material at the precursor [18].

The authors thank S. V. Lebedev for reading of the manuscript and useful comments, V. L. Kantsyrev for help with x-ray diagnostics and B. Le Galloudec for help. Work was supported by the DOE/NNSA under UNR Grant No. DE-FC52-01NV14050. Sandia is a multiprogram laboratory operated by Sandia Corporation, a Lockheed Martin Company, for the U.S. DOE under Contract No. DE-AC04-94AL85000.

-
- [1] C. Deeney *et al.*, Phys. Rev. Lett. **81**, 4883 (1998).
 - [2] T. W. L. Sanford *et al.*, Phys. Rev. Lett. **77**, 5063 (1996).
 - [3] D. B. Sinars *et al.*, Phys. Rev. Lett. **93**, 145002 (2004).
 - [4] S. V. Lebedev *et al.*, Plasma Phys. Controlled Fusion **47**, A91 (2005).
 - [5] B. Jones *et al.*, Phys. Rev. Lett. **95**, 225001 (2005).
 - [6] M. E. Cuneo *et al.*, Phys. Rev. E **71**, 046406 (2005).
 - [7] V. V. Alexandrov *et al.*, JETP **97**, 745 (2003).
 - [8] S. V. Lebedev *et al.*, Phys. Plasmas **8**, 3734 (2001).
 - [9] S. V. Lebedev *et al.*, Phys. Plasmas **9**, 2293 (2002).
 - [10] V. V. Ivanov *et al.*, Phys. Plasmas **13**, 012704 (2006).
 - [11] M. E. Cuneo *et al.*, Phys. Plasmas **13**, 056318 (2006).
 - [12] C. J. Garasi *et al.*, Phys. Plasmas **11**, 2729 (2004).
 - [13] B. Jones *et al.*, Phys. Plasmas **13**, 056313 (2006).
 - [14] M. G. Haines, IEEE Trans. Plasma Sci. **30**, 588 (2002).
 - [15] G. S. Sarkisov *et al.*, JETP **81**, 743 (1995).
 - [16] V. V. Ivanov *et al.*, IEEE Trans. Plasma Sci. (to be published).
 - [17] E. M. Lifshitz, L. D. Landau, and L. P. Pitaevskii, *Electrodynamics of Continuous Media* (Pergamon, Oxford, 1984).
 - [18] S. N. Bland *et al.*, in *The Effect of Wire Initiation on Array Dynamics*, edited by Jeremy Chittenden, AIP Conference Proceedings No. 808 (AIP, New York, 2006).